Mathematical Modeling of Blood Flow Alteration in Microcirculatory Network Due to Angiogenesis

N. O. Gorodnova[1*], A. V. Kolobov[1,2], O. A. Mynbaev[1,3***], and S. S. Simakov[1,3****]**

(Submitted by A. V. Lapin)

[1]*Institute of Numerical Mathematics, Russian Academy of Sciences, ul. Gubkina 8, Moscow, 119333 Russia*

[2]*P.N. Lebedev Physical Institute, Russian Academy of Sciences, Leninskii pr. 53, Moscow, 119991 Russia*

[3]*Moscow Institute of Physics and Technology, Institutskii per. 9, Dolgoprudny, 141707 Russia*

1. INTRODUCTION

A new type anticancer chemotherapy, introduced in 1971 by Folkman [1] and targeting cancer angiogenesis pathways, has been extensively developing during last two decades. Unlike classical chemotherapy, when both tumor and normal cells should be killed, antiangiogenic agents are not aimed to destroy actively dividing cells. Antiangiogenic drugs are expected to initiate arrest of tumor-related angiogenesis in order to inhibit tumor growth by metabolites and oxygen deprivation. As glucose and oxygen (O_2) are considered to be the key metabolites of cell functioning, they are essential also for tumor cell growth. O_2 is an energy nutrient, whereas glucose is energy and basic plastic nutrient. In turn, tumor cells are hypoxic due to their fast growing behavior and exhibit high consumption rate of nutrients. They produced biologically active substances aimed to recruit surrounding cells, known as tumor associated cells, in order to create an optimal environment for tumor cells survival and growth. One of the key ingredients, produced by tumor cells, is a vascular endothelial growth factor (VEGF), which is the key molecule in the angiogenesis pathway. As a result the density of the capillary network surrounding the tumor is increased, which means increase of effective permeability for blood flow and associated increase of O_2 and glucose transport to the tumor. Quantification of these alterations is still underestimated.

Arterio-venous partial pressure gradient of the glucose in blood is relatively small. Maximum value of 12% is achieved in brain tissue. It means that glucose partial pressure along some chosen capillary is almost constant. Thus, the main limiting factor for the glucose delivery to the tissue is the surface area of the capillaries. O_2 arterio-venous partial pressure gradient in blood is always near 100%. Consequently, O_2 consumption rate is much higher than that for glucose. Amount of O_2 available for consumption in the tissue is strongly associated with the number of erythrocytes capable to carry it within the blood flow. Thereby, in contrast to the glucose, O_2 delivery to the tissue is limited by volumetric blood flow.

Total surface of new capillaries formed due to tumor angiogenesis can be assessed on the basis of their number. Blood flow alteration assessment in capillary network with new capillaries is not so obvious it depends on many factors and should be simulated. Such a model may help to predict and explain to understand nutrients delivery rate to the tumor due to angiogenesis. It may help to assess the rate of

[*]E-mail: `Gorodnova@crec.mipt.ru`
[**]E-mail: `Kolobov@lpi.ru`
[***]E-mail: `ospAnmynbaev@hotmail.com`
[****]E-mail: `Simakov.ss@mipt.ru`

glycolysis and glucose oxidation phosphorylation in malignant cells. This is very important for design new anticancer drugs, which are sensitive to the metabolic changes in malignant cells [2].

Blood flow in microcirculatory bed is very complex process. Major physiological factors of microcirculation include non-Newtonian properties of the blood, blood viscosity dependence on capillary diameter (Fahraeus−Lindqvist effect), erythrocytes concentration decrease due to capillary diameter decrease (Fahraeus effect), complex topology of the microvascular network.

Mathematical modeling of the microcirculation is performed by a number of different approaches. In the first approach blood is considered as monophase Newtonian fluid. Poiseuille law relating pressure drop and volumetric flow is used for every microvessel. The network flow is established by extending this condition with mass conservation in the nodes [3]. The second approach treats the blood as two-phase 2D Newtonian fluid separated by two zones: main stream of erythrocytes and boundary layer of cytoplasm [4]. Such models are useful for detailed flow analysis in single capillary. The third approach takes into account blood viscosity dependence on the microvessel's diameter and dependence on erythrocytes concentration. The main variable of the model is hematocrit [6].

Detailed simulations of microcirculation in macro region of a tissue are rarely performed due to complexity of it's structure and great number of elements. 2D model of fluid flow through porous media was proposed to study microcirculatory perfusion at organ scale [7]. This model was coupled with the the network model of large vessels and used for numerical study of global matter transport [8]. Recent micro CT study [9] allows develop and partly validate a model of microcirculation in macro region. In this work we use statistics from the [9] to fit the network parameters.

The paper is organised as follows. In Section 2 we propose a method of the microvascular network structural prototype generation in the case of normal microcirculation and in the case of angiogenesis. In Section 3 a model of blood flow in microvessel's network is presented and it's numerical implementation is discussed. In Section 4 we validate the model of microcirculation by testing relative blood perfusion in healthy case without angiogenesis. In the second part of this section volumetric blood flow alteration due to angiogenesis is analysed. In Section 5 discussion of the model and future perspectives is given.

2. STRUCTURAL MODEL OF MICROCIRCULATORY NETWORK

2.1. Healthy Microcirculation

Structure of the normal microcirculatory network is quite complex. It characterized by extremely high density of small vessels per unit volume. Experimental study of such structure is rarely possible and complicated. Precise experimental *in vivo* study of its structure became available only last decade by means of micro CT and met with difficulties [9].

In this section we propose a method of generation a network structure which can be considered as physiologically correct prototype of the real microcirculatory network. It means that this artificial network may be different from real one but it has the same topology (connectivity), geometrical characteristics (length and diameters distribution, 3D space layout) and functional properties (blood flow permeability per unit volume). In this section we address to the first two aspects (topology and geometrical characteristics). The third aspect (permeability) is considered in Section 4.1 as validation of the model functioning.

Our algorithm consists of two stages. At the first stage a framework of the network is generated, which is composed of small arterioles and venules prototypes. Every node of the framework beside the predetermined inputs and outputs has a number of incident edges between 1 and 3. Coordinates of all nodes (micro-vessel junctions) are randomly generated within predetermined cube in 3D space. At the second stage we apply directed force algorithm of graph layout in 3D space. Finally the network is extended by capillaries prototypes which may connect arterioles and venules or other capillaries.

At the first stage we perform following steps:

(1) A 3D cube is divided to a number of 3D cells by uniform partition in each direction. The number of cells is equal or more than the number of microvessel's connection points (nodes).

(2) Every connection node is placed in separate cell by random uniform distribution along coordinates inside the cell.

(3) Nodes are connected with each other so that directed graph is produced. Every node of the graph has a number of incident edges between 1 and 3. The following limitations are applied. The only node
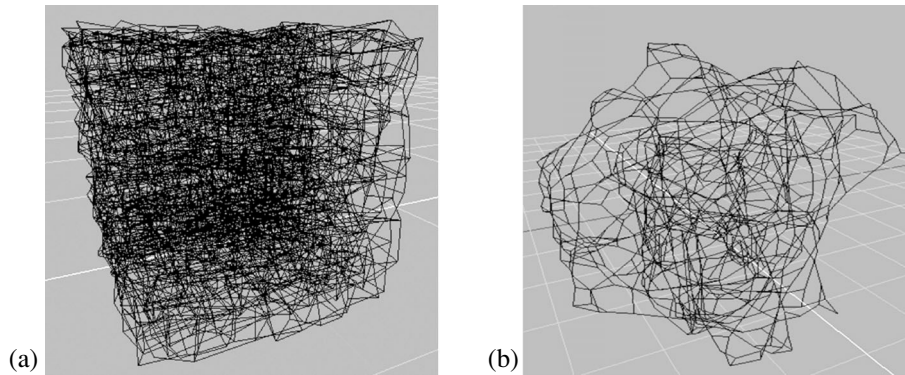
Fig. 1. Capillary network prototype: a—random nodes placement, b—physiologically correct equivalent.

has one outgoing edge. It corresponds to the input. Limited number of nodes (one in most cases) have one incoming edge. These nodes correspond to the output. Possibly nearest nodes are used to set up the edge. One possible output of this step is shown at Fig. 1a.

(4) The edges of the produced network are considered as arterioles and venules structural prototypes. The length and diameter are set up as attributes to each edge according measured distribution [9]. We assume correlation between length and diameter. It means that the edge of greater length has greater diameter value. Actual lengths of the edges do not correspond to the parametric length at this stage. Actual length is updated at the next stage.

Physiologically correct nodes placement in 3D space is achieved by applying Directed Force Layout algorithm to the graph produced at the first step. Review and basic idea of this method can be found in [16]. Energy function should be constructed for a graph which is considered as mechanical system. It is assumed, that every node of the graph produces repulsive force which is exerted to all other nodes and attractive force which is exerted to every node connected by an edge. Repulsive force is commonly inversely proportional to the distance between the nodes. Attractive force is commonly proportional to the distance between the nodes. It may have negative value and become repulsive provided that distance between connected nodes (spatial length of the edge) is less than parametric length. Finally, spatial distribution of the nodes corresponding to the minimum total energy of the system should be produced. Equivalently, spatial distribution of the nodes should be found which gives zero net force for the system. This task can be considered as generalized n-body problem.

Let's define $\mathcal{G}$ as a set of nodes of the graph and $\mathcal{P}$ as a set of node pairs connected by an edge. Let's define unit vector $\mathbf{r}_{uv}$ as

$$\mathbf{r}_{uv} = \frac{\mathbf{r}_v - \mathbf{r}_u}{l_{uv}}, \quad u, v \in \mathcal{G},$$

where $\mathbf{r}_u, \mathbf{r}_v$ are directing vectors of the nodes $u, v \in \mathcal{G}$ and $l_{uv} = ||\mathbf{r}_v - \mathbf{r}_u||$ is an euclidean distance between nodes u and v.

It is not necessary to consider explicit mechanical spring/electric analogy as we only interested in final result of the directed force layout algorithm which should provide relatively uniform distribution of the nodes in 3D space and possibly fit the distances between the connected nodes to the desired length which was set up initially as attribute. Thus logarithm and inverse square dependencies were chosen for attraction and repulsion as they provide faster convergence then conventional spring/electric analogy.

Attractive force from node v to node u is defined as

$$\mathbf{f}_{atr,v}^u = c_{atr} \ln \frac{l_{uv}}{l_{uv}^0} \mathbf{r}_{uv}, \quad (u, v) \in \mathcal{P},$$

where c_{atr} is attractive force coefficient, l_{uv}^0 is the desired length ascribed to the edge as a parameter at previous stage of the algorithm. Repulsive force from node v to node u is defined as

$$\mathbf{f}_{rep,v}^u = -\frac{c_{rep}}{l_{uv}^2} \mathbf{r}_{uv}, \quad u \neq v, \quad v \in \mathcal{G},$$
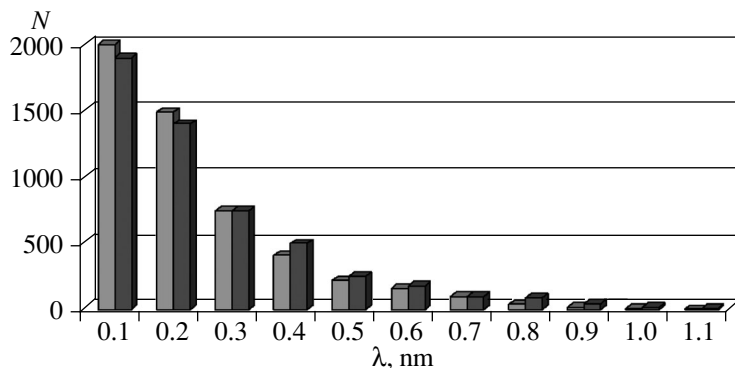
Fig. 2. Vessels distribution by length: comparison between micro CT measurements from [9] and simulated network. N is number of vessels.
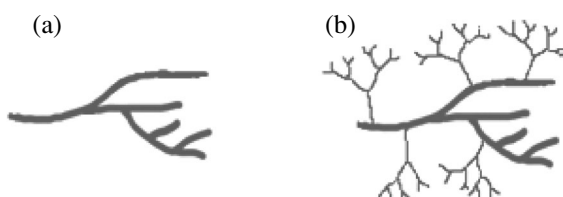

Fig. 3. a—fragment of the basic network, b—example of capillary network elements attachment.

where c_{rep} is repulsive force coefficient. In this work we use $c_{atr} = 0.1, c_{rep} = 0.01$. The net force to the selected node u is calculated as

$$\mathbf{F}^u_{res} = \sum_{(u,v)\in\mathcal{P}} \mathbf{f}^u_{atr,v} + \sum_{v\neq u,v\in\mathcal{G}} \mathbf{f}^u_{rep,v}.$$

Equilibrium state of this system should be found, which means that the following nonlinear equation set should be solved $\mathbf{F}^u_{res} = 0 \quad \forall u \in \mathcal{G}$.

Simple iteration method with relaxation parameter is used to update coordinates of the nodes. New directing vector $\mathbf{r}^{i+1}_u$ of a node u is calculated as

$$\mathbf{r}^{i+1}_u = \mathbf{r}^i_u + \tau\mathbf{F}^{u,i}_{res}.$$

In this work we use $\tau = 0.01$. Maximum number of iterations was set to 10^4 for all cases. Iterations were terminated when 10% error achieved in the length distribution (e.g. see Fig. 2).

One possible result of the algorithm is presented at Fig. 1b. The quality of the algorithm output is confirmed by fitting the vessels distribution by length with experimental data from [9]. The result of such comparison for the case presented at Fig. 1b is shown at Fig. 2.

The network of arterioles and venules is extended with capillaries. We aggregate capillaries to the typical capillary network element. These elements are randomly attached to the edges of arterioles and venules as shown at Fig. 3.

Let's define blind node as a node having 1 incident edge. Each blind end of capillaries originated from arterioles is connected to the nearest blind node of capillaries originated from venules and having 1 incident edge. Thus all such junctions have 2 incident edges.

Capillary diameter is set up randomly from 6 to 10 micron as an attribute. Capillary length is calculated basing on the actual space position of it's nodes. It ranges from $0.4\,mm$ to $1\,mm$ in all structure simulations. The distance between capillaries varies from $0.1\,mm$ to $0.2\,mm$.

2.2. Angiogenesis in Microcirculatory Network

One of the main factors of angiogenic capillary growth is concentration of the VEGF in tissue. In this work we consider uniform space distribution of VEGF. Thus new capillary may be developed anywhere in the network with random uniform distribution. New capillary is attached by one of its nodes to the edge of some pre-existing capillary, which is selected by random uniform distribution. The other node is attached to the edge of another capillary. The second pre-existing candidate is selected by random uniform distribution basing on the limitation that new capillary length should be not more than $4\,mm$. This is always possible as the distance between pre-existing capillaries varies from $0.1\,mm$ to $0.2\,mm$ as mentioned in Section 2.1.

3. BLOOD FLOW MODEL IN MICROCIRCULATORY NETWORK

Blood flow in microcirculatory region is substantially different form the one in large vessels. The flow is stationary without pulsations. The driving force is applied due to pressure drop between input and outputs. Blood composition and rheology is also important factor. Thus for every microvessel indexed as uv we use Poiseuille's law for pressure drop in the form

$$Q_{uv} = G_{uv}\left(P_v - P_u\right), \quad (u,v) \in \mathcal{P}, \tag{1}$$

and mass conservation condition in the selected node u in the form

$$\sum_{(u,v)\in\mathcal{P}} Q_{uv} = 0, \tag{2}$$

where G_{uv} is conductivity coefficient, Q_{uv} is volumetric blood flow, P_u, P_v are pressures in the nodes u and v, R_{uv} is radius, μ is blood viscosity,

$$G_{uv} = \frac{8\mu l_{uv}}{\pi R_{uv}^4}. \tag{3}$$

At the input and outputs of the network constant pressure values were set according to the physiological values $P^{in} = 35$ mm Hg, $P^{out} = 20$ mm Hg. The set (1)–(3) is a set of linear equations. It is solved by the following iteration procedure

$$P_u^{i+1} = \frac{\displaystyle\sum_{(u,v)\in\mathcal{P}} P_v^i G_{uv}}{\displaystyle\sum_{(u,v)\in\mathcal{P}} G_{uv}}, \quad u \in \mathcal{G}.$$

The flow is than updated as

$$Q_{uv}^{i+1} = G_{uv}\left(P_v^{i+1} - P_u^{i+1}\right), \quad (u,v) \in \mathcal{P}.$$

Initial pressure in all internal nodes was set as $P_u^0 = 0$ mm Hg. Maximum number of iterations was set to 3×10^4. Iterations were terminated when 0.1% relative error achieved in pressure values at all nodes between two successive iterations.

4. RESULTS

4.1. Relative Blood Perfusion in Healthy Microcirculation

Functional validation of the model was performed using analysis of relative blood perfusion per unit volume. Normal capillary network should provide uniform distribution of this parameter.

The result of microcirculatory network prototype structure simulation represents spherical-like 3D space layout of the network (see Fig. 1b). Spherical region is divided into a number of spherical layers. External radius of the nth layer is set as

$$r_n = \frac{n}{N}R_N, \quad n = 1,\ldots,N, \tag{4}$$

where n is index of spherical layer, R_N is radius of the embracing sphere, N is number of layers.
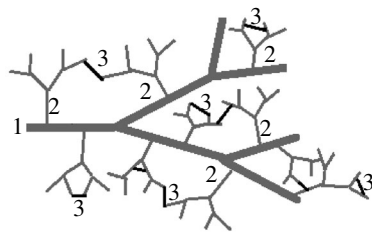
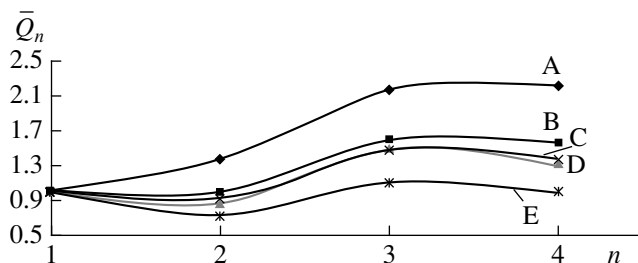**Fig. 4.** Scheme of new capillaries generation. 1—arterioles or venules, 2—normal capillaries, 3—new capillaries.

Fig. 5. Averaged relative unit blood perfusion by number of microvessels. A—18×10^3, B—21×10^3, C—24×10^3, D—30×10^3, E—37×10^3.

Unit blood perfusion was calculated for every spherical layer as a ratio of total blood flow in the vessels of the region to the volume of this region. Unit blood perfusion of the first layer $(0 < r < r_1)$ which also is a sphere of radius r_1 was selected as reference value for relative unit blood perfusion analysis. Thus, we define $\bar{Q}_1 = 1$. Relative unit blood perfusion $\bar{Q}_n$ can be calculated as

$$\bar{Q}_n = \frac{Q_n/V_n}{Q_1/V_1}, \quad n = 1, \ldots, N,$$

where Q_n total blood flow in the nth layer, V_n volume of the nth layer. In the ideal case relative unit blood perfusion $(\tilde{Q})$ is constant $(\tilde{Q}_n = 1, \, n = 1, \ldots, N)$. It means absolutely uniform blood supply of the tissue.

In this work we set $R_N = 0.6$ cm, $N = 6$. Five series of computational experiments were carried out for the total number of microvessels in m^{th} case $K_m \in \{18 \times 10^3, 21 \times 10^3, 24 \times 10^3, 30 \times 10^3, 37 \times 10^3\}$, $m = 1, \ldots, 5$. The value $K_5 = 37 \times 10^3$ corresponds to the physiological density of the microvessels per unit volume for sphere of radius $R_N = 0.6$ cm. It was considered 10 different randomly generated networks by algorithm presented in Sec. 2.1 for every K_m. Blood flow distribution was calculated by algorithm presented in Section 3. Relative unit blood perfusion was averaged in each case. Results are shown at Fig. 5. From Fig. 5 is clear that the networks composed by relatively small number of the microvessels can't provide uniform supply of the tissue. An increase of the microvessels number and, thus, density per unit volume results in more uniform volumetric supply. Physiologically acceptable number and density of the microvessels allows to generate networks with almost uniform volumetric perfusion.

Mean square deviation from ideal case is presented in table 1. It was calculated as

$$\sigma_n^m = \frac{1}{\sqrt{5}} \left(\sum_{i=1}^{5} \left(\bar{Q}_n^i - \tilde{Q}_n \right) \right)^{1/2}, \quad m = 1, \ldots, 5, \quad n = 1, \ldots, 6.$$

Obviously, for any network $\sigma_1^m = 0$, so the first segment is not included. The stable decrease of σ_n^m with increase of m and regardless of $n = 2, \ldots, 4$ confirm that increased number of microvessels up to physiologically reasonable value allows to generate networks with required functional properties.

From Table 1 it is also clear, that mean square deviation from ideal case remains extremely high in the external layers even for dense networks. This is principal limitation of our approach. Real microvascular

Table 1. Mean square deviation of relative blood perfusion from ideal perfusion. K_m is number of microvessels, n is index of segment according to (4)

K_m	n				
	2	3	4	5	6
18×10^3	0.54	1.75	1.87	0.73	0.9
21×10^3	0.46	1.07	1.02	0.59	0.97
24×10^3	0.29	0.69	0.85	0.68	0.98
30×10^3	0.26	0.59	0.46	0.69	0.99
37×10^3	0.28	0.15	0.12	0.71	0.99

Table 2. Standard deviation of relative blood perfusion. K_m is number of microvessels, n is index of segment according to (4)

K_m	n				
	2	3	4	5	6
18×10^3	0.18	1.77	2.60	0.44	0.00
21×10^3	0.21	0.77	0.76	0.07	0.00
24×10^3	0.06	0.27	0.60	0.07	0.00
30×10^3	0.06	0.29	0.32	0.01	0.00
37×10^3	0.00	0.06	0.01	0.00	0.00

network has very complicated connectivity. It has many inputs and outputs so that it is impossible to isolate autonomous region, which is supplied by one input arteriole.

Standard deviation is presented in Table 2. Substantial distinct decrease of standard deviation in all segments is observed with increase of the number of microvessels up to physiological conditions. It means that result of random network generation by our algorithm become more stable if the number of microvessels is taken from the physiological rage. The other conclusion from Table 2 is stable failure in simulating relative unit perfusion in the external layers. It confirms principal limitation of this approach. Also, it confirms correct blood flow simulation in the core region of the network.

Computational experiments of this section confirm that it is still possible to simulate blood flow by our method in isolated region of microcirculation saving the most important physiological features. Our analysis shows that internal spherical region of radius $\tilde{R}_N = 2R_N/3$ (approximately 70% of total volume) can be adequately simulated regardles of $N > 6$ for $R_N = 0.6$ cm. Thus the network in the region $\tilde{R}_N < r < R_N$ should be excluded from the analysis. But it plays important role as a boundary layer maintaining correct boundary conditions and blood flow in the rest of the network.

4.2. Blood Perfusion Alterations Due to Angiogenesis

It is well known that the microcirculatory network transforms during angiogenesis process. New capillaries are formed depending on VEGF concentration in the tissue. Algorithm of microcirculatory network update during angiogenesis (see Section 2.2) is used in this section to account for this feature and for analysis of blood perfusion alterations depending on capillary network density increase due to angiogenesis.

Tumor induced angiogenesis is supposed to increase O_2 supply of neoplasm and surrounding normal tissue. Oxygen transport depends on the number of erythrocytes and, thus, on volumetric blood flow through microcirculatory network. According to Poiseuille law volumetric blood flow depends on pressure drop and permeability of the region. In the considered case pressure drop between
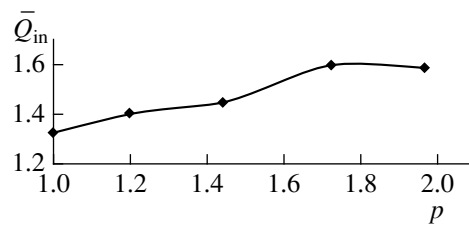
Fig. 6. Volumetric blood flow in afferent arteriole (mm^3/s) depending on the relative increase of capillaries.

afferent arteriole and draining venules is constant in wide range of conditions. It depends on general arteriovenous pressure drop, which is determined by systemic haemodynamics. Thus, volumetric blood flow alteration depends on effective permeability of microcirculatory network, which, in turn, determined by density and structure of capillary network consisted of pre-existing and new capillaries formed due to angiogenesis.

Calculated alterations of volumetric blood flow in afferent arteriole is present at Fig. 6. Blood flow was simulated for different capillary network density and uniform distribution in the region of interest. Greater microcirculatory density is associated in the model with higher level of tumor induced angiogenesis in tissue. Total number of capillaries is described by parameter p

$$p = \frac{N_0 + N_{angio}}{N_0},\tag{5}$$

where N_0 is a number of capillaries in normal network (without angiogenesis), N_{angio} is a number of new capillaries developed due to tumor induced angiogenesis. We consider a range of p from 1 (normal network) to 2. The upper value is limited by the space available in tissue for new capillaries.

From Fig. 6 one may observe an increase of volumetric blood flow in afferent arteriole up to 20% during maximum possible angiogenesis. It may results in substantial change of O_2 supply of the tumor up to 20%. This value may differ depending on structural, flow and angiogenesis models complexity. In the present case it demonstrates substantial contribution of angiogenesis to the O_2 supply increase. Alterations of the volumetric blood flow in afferent arteriole due to angiogenesis is very important characteristic for further development of the joint model of tumor growth [17] and its nutrients supply by blood flow.

5. DISCUSSION

The results obtained in this study indicate that tumor angiogenesis is more conducive to the influx of glucose, whereas increase of O_2 inflow is rather small. Figure 9 clearly shows that two-fold increase in the density of the capillary network leads to only $20-25\%$ increase of blood flow therethrough, and thus the inflow of O_2 into the tissue will grow in a similar manner. At the same time, the similar increase of capillary network density will twice increase the inflow of glucose into angiogenic tissue.

It should be emphasized that the change in the ratio between the supply of glucose and O_2 to the tissue as a result of angiogenesis should lead to a change in the ratio between glucose oxidation phosphorylation and glycolysis in energy production of malignant cells, in favor of the latter. Experimentally, it is the first time found Otto Warburg in 1956 [18]. Thus glycolysis prevails in energy tumor cells even in the presence of excess O_2 concentration, which was originally called by Warburg "fermentation", the process is currently better known as "aerobic glycolysis" [2]. In light of our results one possible explanation for such a transformation of malignant cells may be occurring due to angiogenesis skewed influx of glucose in the tumor growth, which is grafted to the predominance of the tumor cells with the preferred mechanism for glycolytic energy production. However, this issue requires a separate study.

In this work we accepted a number of simplifications which should be subjected to more detailed analysis in the future. In the case of tumor angiogenesis VEGF concentration is not uniform in space. A model of tumor growth is required (e.g. [17]) for realistic assessment of VEGF distribution. The other important structural feature is that pre-existing as well as new capillaries should degenerate non uniformly in necrotic zone of the tumor.

Viscosity factor in microvessels substantially depends on hematocrit factor, diameter and volumetric blood blow. It gives nonlinear dependency in (3) and, thus, in mass conservation equations (2). All these aspects should be taken into account in future work.

Nevertheless, the model developed in this work, may be used for fast but physiologically correct preliminary assessment of blood flow alteration in the microcirculatory region due to angiogenesis. The method of microcirculatory structural prototype generation steadily produces networks providing almost uniform relative perfusion per unit volume. A tissue sample of volume up to 1 cm^3 and containing up to 10^5 microvessels can be simulated. Such microvessels concentration per unit tissue volume is in physiologically acceptable range. The network flow distribution also may be used as null approximation for a more complex nonlinear models, which should improve convergence of iterations in their numerical implementations.

ACKNOWLEDGMENTS

REFERENCES

1. J. Folkman, "Tumor angiogenesis: therapeutic implications," N. Engl. J. Med. **285**, 1182−1186 (1971).
2. F. Bost, A.-G. Decoux-Poullot, J. F. Tanti, and S. Clave, "Energy disruptors: rising stars in anticancer therapy?" Oncogenesis **5**, e188 (2016).
3. S. K. Stamatelos et al., "A bioimage informatics based reconstruction of breast tumor microvasculature with computational blood flow predictions," Microvascular Research **91**, 8−21 (2014).
4. J. E. Fletcher, "Mathematical modeling of the microcirculation," Mathematical Biosciences **38** (3), 159−202 (1978).
5. V. P. Srivastava, "A theoretical model for blood flow in small vessels," Applications and Applied Mathematics **2** (1), 51−65 (2007).
6. J. B. Geddes et al., "Blood flow in microvascular networks: a study in nonlinear biology," Chaos: An Interdisciplinary Journal of Nonlinear Science **20** (4), 045123 (2010).
7. A. S. Kholodov, A. V. Evdokimov, and S. S. Simakov, "Numerical simulation of peripheral circulation and substance transfer with 2D models," in *Mathematical Biology: Recent Trends*, Ed. by P. Chandra and R. Kumar (Anamaya, 2006), pp. 22−29.
8. A. S. Kholodov, S. S. Simakov, A. V. Evdokimov, and Y. A. Kholodov, "Matter transport simulations using 2D model of peripheral circulation coupled with the model of large vessels," in *Proceedings of II International Conference On Computational Bioengineering*, Ed. by Rodrigues H. et al. (IST Press, 2005), Vol. 1, pp. 479−490.
9. S. K. Stamatelos, E. Kim, A. P. Pathak, and A. S. Popel, "A bioimage informatics based reconstruction of breast tumor microvasculature with computational blood flow predictions," Microvascular Research **91**, 8−21 (2014).
10. Su Shen-Wei, M. Catherall, and S. Payne, "The influence of network structure on the transport of blood in the human cerebral microvasculature," Microcirculation **19** (2), 175−187 (2012).
11. E. M. Renkin and F. E. Curry, "Transport of water and solutes across capillary endothelium," Membrane Transport in Biology **4**, 1−45 (1979).
12. L. J. Rodney, *An Introduction to Cardiovascular Physiology* (Butterworth-Heinemann, 2013).
13. M. Konerding, C. Van Ackern, E. Fait, F. Steinberg, and C. Streffer, "Morphological aspects of tumor angiogenesis and microcirculation," in *Blood Perfusion and Microenvironment of Human Tumors* (Springer-Verlag, Berlin, 1998), pp. 5−17.
14. E. M. Renkin, "Filtration, diffusion, and molecular sieving through porous cellulose membranes," The Journal of General Physiology **38** (2), 225−243 (1954).
15. E. M. Renkin, "Multiple pathways of capillary permeability," Circulation Research **41** (6), 735−743 (1977).
16. S. Simakov, I. Ispolatov, S. Maslov, and A. Nikitin, "Algorithmic basis for pathway visualization," in *Pathway Analysis for Drug Discovery: Computational Infrastructure and Applications* (Wiley, 2008).
17. A. V. Kolobov and M. B. Kuznetsov, "Investigation of angiogenesis influence on tumor growth rate. Analysis by mathematical modeling," Biophysics **60** (3), 555-563 (2015).
18. O. Warburg, "On the origin of cancer cells," Science **123**, 309−314 (1956).